Journal of Environmental Chemical Engineering 12 (2024) 113110

Contents lists available at ScienceDirect

Journal of Environmental Chemical Engineering

journal homepage: www.elsevier.com/locate/jece

Influence of the TiO_2 crystalline phase on the performance of UVA/brookite/persulfate and UVA/anatase/persulfate systems for the degradation of isothiazolinones in aqueous matrices

P. Gómez-Rodríguez [a], R. van Grieken [a,b], M.J. López-Muñoz [a,b,*]

[a] Chemical and Environmental Engineering Group, Departamento de Tecnología Química y Ambiental, ESCET, Universidad Rey Juan Carlos, C/Tulipán s/n, Móstoles 28933, Spain

[b] Instituto de Tecnologías para la Sostenibilidad, Universidad Rey Juan Carlos, C/Tulipán s/n, Móstoles 28933, Spain

ARTICLE INFO

Keywords:
Isothiazolinones
TiO_2-brookite/anatase photocatalysis
Persulfate activation
Secondary effluent water matrix

ABSTRACT

The activation of persulfate (PS) under UVA irradiation by two TiO_2 polymorphs (brookite and anatase) and titanate photocatalysts was evaluated for the simultaneous removal of the biocides methylisothiazolinone (MIT) and chloromethylisothiazolinone (CMIT), in ultrapure water and real sewage treatment plant water (SW). Titania and titanate samples were synthesized by a hydrothermal method and characterized by XRD, SEM, N_2 adsorption-desorption isotherms and UV-Vis DR. The reactions were performed in individual (brookite, anatase, titanate and PS) and hybrid (titania/PS and titanate/PS) systems and compared to those with TiO_2-P25 as reference. In ultrapure water, the combined brookite/PS system showed a higher performance for MIT and CMIT abatement and a stronger synergistic effect between titania and PS than found in anatase/PS and titanate/PS systems, indicating the higher effectiveness of the brookite phase for PS activation under UVA. The use of SW water revealed the strong inhibitory effect of matrix constituents in the individual brookite, anatase and PS systems, which exhibited a low performance. However, the kinetics of MIT/CMIT in SW were greatly enhanced in the hybrid TiO_2/PS systems, especially with brookite, leading to an efficient degradation of both pollutants and the decrease of total organic carbon (TOC). The addition of chemical scavengers showed a similar reactivity of $HO^{\bullet}$ towards both isothiazolinones whereas a preferential attack of $SO_4^{\bullet-}$ to MIT was observed, demonstrating the selective nature of $SO_4^{\bullet-}$.

1. Introduction

The ability of sulfate radicals ($SO_4^{\bullet-}$) to oxidize pollutants in water and wastewater systems has received increasing attention in recent years because, compared to hydroxyl radicals ($HO^{\bullet}$), $SO_4^{\bullet-}$ exhibits a similar standard redox potential (E^0 ($HO^{\bullet}/OH^-$) = 2.8 V *vs.* NHE; E^0 ($SO_4^{\bullet-}/SO_4^{2-}$) = 2.6 V *vs.* NHE) but better stability and higher selectivity [1]. $SO_4^{\bullet-}$ can be formed through the activation of peroxydisulfate (PS, $S_2O_8^{2-}$) or peroxymonosulfate (PMS, HSO_5^-) salts by different methods, including the input of energy (UV, heat, microwave, or ultrasound), alkali treatment, and the use of transition metals and metal oxides [2]. As an alternative for promoting the activation of persulfate, the assistance by heterogeneous photocatalysis has been recently proposed [3]. The fundamentals of heterogeneous photocatalysis are well known since this process has been widely investigated. TiO_2 is the photocatalyst most commonly used because of its great ability to achieve the degradation of inorganic and organic compounds, as well as its good thermal and chemical stability, low cost, and non-toxicity. When TiO_2 is exposed to UVA irradiation, it can absorb the photons whose energy overcomes its bandgap energy level. This leads to the migration of electrons from the valence band (VB) to the conduction band (CB) of the semiconductor (e_{CB}^-), resulting in the generation of positive holes (h_{VB}^+) in the VB [4]. Following their generation most e^--h^+ pairs recombine with release of energy but if suitable charge carrier acceptors are available, electrons and holes will be trapped resulting in the formation of reactive species such as superoxide radical anions ($O_2^{\bullet-}$) (Eq. (1)), and hydroxyl radicals ($HO^{\bullet}$) (Eq. (2)). In presence of PS or PMS, e_{CB}^- can accomplish the activation of PMS and PS, producing $SO_4^{\bullet-}$ (Eqs. (3) and (4)) [5], which also

* Corresponding author at: Chemical and Environmental Engineering Group, Departamento de Tecnología Química y Ambiental, ESCET, Universidad Rey Juan Carlos, C/Tulipán s/n, Móstoles 28933, Spain

E-mail address: mariajose.lopez@urjc.es (M.J. López-Muñoz).

https://doi.org/10.1016/j.jece.2024.113110
Received 27 December 2023; Received in revised form 14 May 2024; Accepted 17 May 2024
Available online 19 May 2024

prevents the charge carriers recombination hence favoring the photocatalytic process. In addition, it has been reported that $S_2O_8^{2-}$ can react with $O_2^{\bullet-}$ to produce more sulfate radicals (Eq. (5)) [6] whereas $SO_4^{\bullet-}$ can also react with HO^- generating $HO^\bullet$ in water solution under alkaline conditions (Eq. (6)):

$$O_2 + e_{CB}^- \rightarrow O_2^{\bullet-} \quad (1)$$

$$H_2O + h_{VB}^+ \rightarrow HO^\bullet + H^+ \quad (2)$$

$$HSO_5^- + e_{CB}^- \rightarrow SO_4^{\bullet-} + HO^- \quad (3)$$

$$S_2O_8^{2-} + e_{CB}^- \rightarrow SO_4^{\bullet-} + SO_4^{2-} \quad (4)$$

$$S_2O_8^{2-} + O_2^{\bullet-} \rightarrow SO_4^{\bullet-} + SO_4^{2-} + O_2 \quad (5)$$

$$SO_4^{\bullet-} + HO^- \rightarrow HO^\bullet + SO_4^{2-} \quad (6)$$

In nature, TiO_2 can crystallize as three different polymorphs: anatase (tetragonal, $I4_1/amd$), rutile (tetragonal, $P4_2/mmm$), and brookite (orthorhombic, P_{bca}). All of them are composed of distorted TiO_6 octahedra with a distinctive arrangement, which gives rise to different optical and textural properties in each polymorph [7]. Consequently, the crystalline phase plays a key role in the photocatalytic activity of the semiconductor. Anatase and rutile phases have been so far the most studied, usually being reported a greater activity of anatase than rutile when evaluated as pure phases, and a beneficial synergetic effect when used as a mixture, as it occurs in the commercial TiO_2 P25 [8]. By contrast, TiO_2-brookite has not received so much attention, mainly due to the difficulties in synthesizing this crystalline phase pure [7].

So far, most studies on persulfate-assisted TiO_2 photocatalysis with UVA radiation have been focused on the use of commercial TiO_2 P25 [9]. On this basis, the aim of the present work has been investigating the influence of the titania crystalline phase on the photocatalytic activation of PS for the removal of a mixture of chloromethylisothiazolinone (CMIT) and methylisothiazolinone (MIT) in different water matrices. The combination of both target compounds, commercialized as a mixture of CMIT:MIT in a 3:1 wt. ratio, is widely used in personal care and cleaning products and to prevent biological fouling in reverse osmosis processes due to its high biocide activity. However, their presence in effluents from wastewater treatment plants and natural water, even in low concentration, is a matter of environmental concern due to their toxicity to aquatic organisms [10].

Anatase (A), brookite (B) and titanates (T) samples were synthesized by an alkaline hydrothermal method and their photocatalytic performance in MIT and CMIT degradation was investigated in individual (A, B, T, and PS) and combined systems with persulfate (A/PS, B/PS and T/PS). The synergistic effects of integrated systems were evaluated in ultrapure water and water from the effluent of the secondary treatment of a WWTP. Finally, the involvement of the primary ROS species formed in the different systems was evaluated.

2. Materials and methods

2.1. Chemicals

The stock solutions were prepared in ultrapure water (resistivity 18.2 MΩ·cm, at 25°C) (Milli-Q system). Titanium (IV) butoxide (Ti(C_4H_9O)$_4$, 97%), methanol (MeOH, CH_3OH, ≥99.9%), ethanol (EtOH, C_2H_6O, ≥99.8%,), *tert*-butanol (TBA, $C_4H_{10}O$, ≥99.5%) and ProClin™ 150 (CMIT/MIT mixture in 3:1 ratio) were purchased from Merck. TiO_2-P25 was supplied by Evonik. Ammonia (NH_3, 28%), sodium chloride (NaCl, 99%), potassium chloride (KCl, 99%) and sodium persulfate ($Na_2S_2O_8$, EssentQ®) were supplied by Scharlau.

2.2. Preparation of TiO_2 catalysts

The synthesis of materials was performed following the procedure described in a previous work [11]. Briefly, 0.046 mol of titanium (IV) butoxide were added to 140 mL of an aqueous solution containing 0.0018 mol NH_3 and either NaCl or KCl in the range 0.25–0.50 M. After magnetic stirring for 2 h, the suspension was submitted to hydrothermal treatment at 180 ºC in a Teflon-lined autoclave in the range 24–192 h. The solid obtained was recovered by filtration, washed, and dried at 110 ºC overnight. Table 1 summarizes the notation, specific synthesis variables and main properties of the samples.

2.3. Photocatalytic experiments

The photocatalytic activity of samples was investigated for the degradation of MIT and CMIT in Milli-Q water and water collected from the secondary effluent (SW) of a sewage treatment plant located in Móstoles (Spain). The initial concentrations of CMIT and MIT were set at 75.54 μM and 33.0 μM, respectively, and the catalyst dosage at 0.5 g·L^{-1}. 2 mM of PS was established for persulfate activation experiments, based on a previous work [12]. The reactions were performed in duplicate at natural pH (*ca.* 6) in a Pyrex batch reactor (1 L of effective volume) with a 150 W medium pressure mercury discharge lamp (Heraeus TQ-150), axially immersed in the solution and provided with a cutoff filter for λ<300 nm. During the reaction, the solution was stirred magnetically and bubbled with air. Aliquots (1 mL) were collected and filtered through a 0.45 μm Nylon filter for subsequent analysis by HPLC.

2.4. Analytical procedures

The crystalline phases were identified by powder X-Ray Diffraction (XRD) (Philips X`PERT MPD) with Cu Kα radiation (λ=1.5418 Å) at a scan range of 2θ=5–90 °, a step size of 0.01° and 1 s per step. The crystallite size was calculated by the Scherrer equation. The determination of the surface area (S_{BET}) was carried out according to the Brunauer-Emmett-Teller method determined by N_2 adsorption-desorption isotherms at 77 K on a Micromeritics Tristar3000 instrument. The morphology of the materials was examined by scanning electron microscopy (SEM) with a XL30 ESEM Philips equipment and Nova Nano SEM230 (FEG-SEM). Diffuse reflectance spectra from 200 to 800 nm were obtained with a Cary 5000 UV–vis–NIR spectrophotometer (Agilent) with a scan rate of 100 nm·min^{-1}.

The concentrations of MIT and CMIT were determined using a HPLC-DAD (Agilent 1260 Infinity II) provided with a Poroshell 120 EC-C18 column (4.6 ×100 nm, Ø= 2.7 μm), kept at 24 ºC. The system was equipped with a Diode-Array Detector which operated at 274 nm. The initial conditions of the mobile phase consisted of a 90:10 mixture of acetic acid (0.1% v/v) and methanol at a flow rate of 0.8 mL·min^{-1} in gradient mode. At 10 min, the percentage of each eluent was 70% and 30%. From 10–15 min the mobile phase returned to the initial conditions to stabilize the system before the next injection.

Total organic carbon (TOC) was measured using a Shimadzu TOC-5000 analyzer (catalytic oxidation on Pt/Al_2O_3 quartz reactor at 953 K).

3. Results and discussion

3.1. Catalysts characterization

Based on a previous work [11] the synthesis variables, namely the alkali ion added, its concentration, and the duration of the alkaline hydrothermal treatment were selected (Table 1) to tailor the desired titania phases. Fig. 1 (A) displays the X-ray diffractograms of the synthesized samples. B1 and B2 materials showed the characteristic pattern of pure brookite (JCPDS, No. 29–1360) with the main peaks located at 25.34º, 25.68º and 30.78º, indexed to (120), (111), and (121) diffractions, respectively. The patterns of A1 and A2 samples corresponded to

Table 1
Synthesis conditions, textural and optical properties of TiO_2 and titanate samples.

Sample	Electrolyte	Time of hydrothermal treatment (h)	Phase composition	S_{BET} ($m^2\ g^{-1}$)	Crystallite size (nm)	E_g (eV)
B1	NaCl, 0.25 M	72	B	38.1	34.9	3.27
B2	NaCl, 0.5 M	192	B	16.5	52.4	3.30
A1	KCl, 0.5 M	192	A	44.0	41.4	3.23
A2	None	72	A	36.3	36.5	3.23
T1	KCl, 0.5 M	24	T	190.9	-	3.32
T2	NaCl, 0.5 M	24	T	202.2	-	3.26

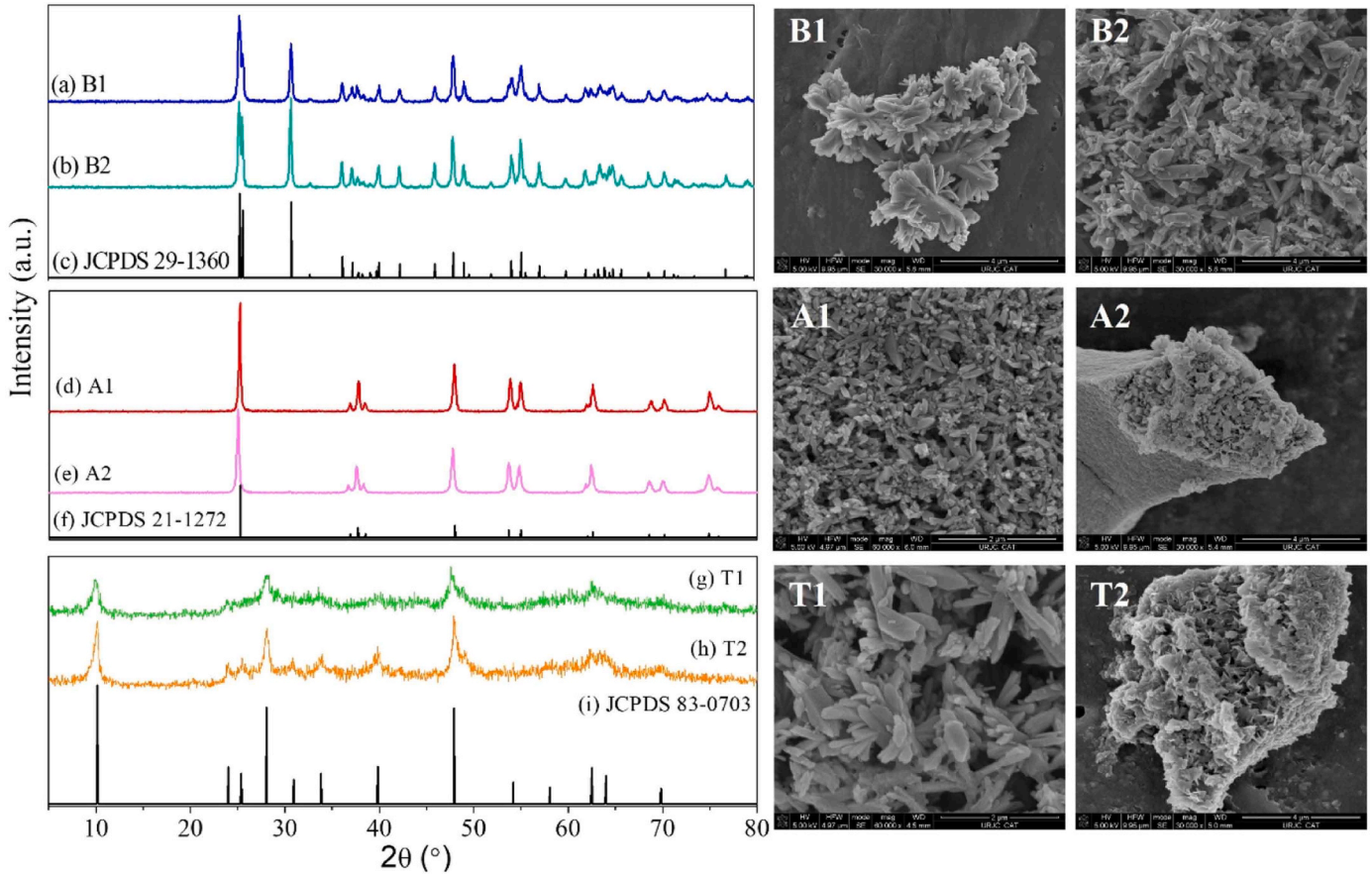

Fig. 1. (A) XRD patterns of synthesized materials. Vertical bars in black denote the standard data for brookite (JCPDS, No. 29–1360), anatase (JCPDS, No.21–1272), and layered titanate (JCPDS, No 83–0703). (B-G) SEM images of B1, B2, A1, A2, T1 and T2 materials.

anatase phase (JCPDS, No. 21–1272), with the main peak centered at 25.27º, indexed to (101). T1 and T2 consisted of layered titanates, with peaks at 9.8º, 24.0º, 28.1º and 48.0º, which correspond to (200), (110), (310) and (020) diffractions, respectively (JCPDS, No. 83–0703). The results show that after 24 h of hydrothermal treatment the titanate structure is stable in presence of both alkali ions, Na^+ and K^+. By contrast, after longer reaction times the nature of the alkali ion plays a significant role on the TiO_2 phase obtained, since Na^+ promotes the formation of brookite phase while K^+ that of anatase phase, in accordance with previous reports [13]. The Scherrer equation was applied to the (121), (101) diffractions of brookite and anatase, respectively, obtaining a similar crystal size for B1 and A2, which increased with the duration of the hydrothermal treatment for both crystalline phases (Table 1). Fig. 1 (B-G) displays some representative SEM images, which show the different morphology of the materials. T1 consists of particles in the range 4–6 μm, formed by aggregation of flake structures with pronounced micaceous cleavage. T2 is formed by a mixture of flakes and rods, most of them of ca. 500 nm size. Brookite B1 consists of rods of ca. 1μm size on which smaller nanorods are aggregated in a flower-like shape. The latter shape disappears by increasing the duration of the treatment (B2), resulting in an agglomerate of submicro-sized nanorods. A1 appears as a heterogeneous mixture of particles (50–100 nm size) and nanorods (200–300 nm size) and A2, consists of bigger particles (50–100 μm size) with an inner content of irregular shaped particles (100–200 nm size). The N_2 adsorption and desorption isotherms (shown in Fig. S1) followed the typical type IV, that correspond to mesoporous materials.

Table 1 displays the specific surface areas (S_{BET}), which are similar for B1, A1 and A2, while significantly higher for T1 and T2. The UV-Vis DR spectra were used for estimating the band gap values (E_g) from the Tauc Plot assuming that the materials were indirect semiconductors (Fig. S2). As observed in Table 1, the E_g values showed no significant differences.

3.2. UVA-assisted degradation of MIT and CMIT with TiO_2, titanate, and PS systems

The degradation of MIT and CMIT was first tested in Milli-Q water.

Preliminary experiments in dark conditions demonstrated no adsorption on the TiO_2 or titanate samples after 60 min. Less than 5% and 9% degradation of MIT and CMIT, respectively, was observed by photolysis. As illustrated in Fig. 2 (A)-(B), P25 showed the best photocatalytic performance, followed by brookite B1. After 60 min of irradiation, 96% and 74% degradation of MIT were achieved with P25 and B1, respectively, while 94% and 74% were observed for CMIT. By contrast, the titanate samples showed a negligible performance. Interestingly, the MIT and CMIT concentration profiles with time were very similar for each titania photocatalyst. Since it is considered that hydroxyl radicals are the main oxidative species formed by TiO_2 [14] this result would indicate a similar reactivity of $HO^{\bullet}$ towards both organic molecules. Next, the disappearance of MIT and CMIT was investigated in the presence of PS both in homogeneous conditions and contemporarily with the tested photocatalysts. Preliminary experiments proved no activity of PS in dark conditions, but under UVA radiation the addition of PS was greatly beneficial for the abatement of MIT and CMIT (Fig. 2 (C)-(D)). In the homogeneous system, the effective degradation of MIT/CMIT can be related to PS photoactivation to generate $SO_4^{\bullet-}$ (Eq. (7)), able to promote the oxidation of the organic molecules [15].

$$S_2O_8^{2-} \xrightarrow{UVA} 2SO_4^{\bullet-} \quad (7)$$

In contrast to the reactions with TiO_2, in the homogeneous PS system the degradation rate was significantly different for MIT compared to CMIT. After 60 min, the concentration of the former was below the detection limit, whereas only 50% degradation of the latter was achieved. The results suggest a different mechanism for the degradation of MIT and CMIT with $SO_4^{\bullet-}$ compared to $HO^{\bullet}$. Even though both radicals can react by i) electron transfer, ii) addition to the unsaturated double bonds, and iii) H abstraction, it is widely accepted that $SO_4^{\bullet-}$ radicals usually react *via* electron transfer reactions while $HO^{\bullet}$ generally undergoes hydrogen-atom abstraction and addition reactions. Thus, despite the similar oxidation potentials of $SO_4^{\bullet-}$ and $HO^{\bullet}$, their respective mechanisms for pollutants degradation can be significantly different, usually being $SO_4^{\bullet-}$-driven oxidation much more selective [16]. Accordingly, it has been reported that the reactivity of $SO_4^{\bullet-}$ toward aromatic compounds is highly sensitive to substituent effects, in contrast to $HO^{\bullet}$. Neta et al. [17] investigated the rate constants of $SO_4^{\bullet-}$ with aromatic compounds and reported that electron-withdrawing

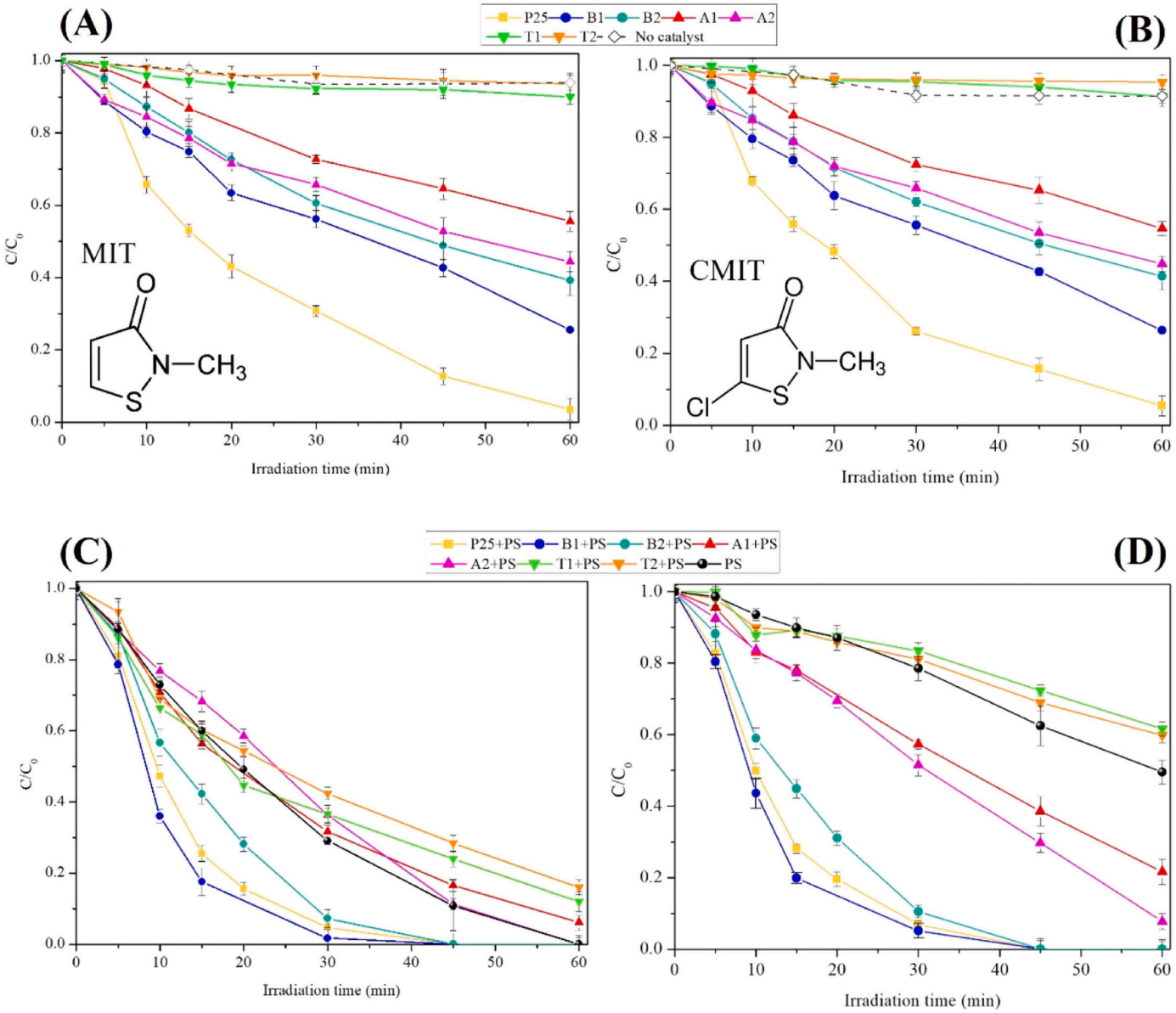

Fig. 2. Photocatalytic degradation of (A) MIT and (B) CMIT without PS addition and (C) MIT and (D) CMIT with PS addition in Milli-Q water.

substituents led to a significant decrease in the rate constant, which was related to the electrophilicity of $SO_4^{\bullet-}$ radicals. Compared to MIT, CMIT is characterized by a Cl substituent located in the C adjacent to the S atom (inset Fig. 2 (A)-(B)). Since $SO_4^{\bullet-}$ are prone to react with electron-rich S atoms to form sulfone products [10], the electron-withdrawing Cl might disfavor the initial attack of $SO_4^{\bullet-}$ on S, thus leading to a slower CMIT degradation rate compared to MIT in the PS homogeneous system.

Fig. 2 (C)-(D) shows that the contemporary use of TiO_2 and PS resulted in a faster degradation rate of CMIT compared to the individual processes. A beneficial effect was also observed for MIT abatement by combining PS with B1, B2 and P25 but not with anatase or titanate materials. The time-dependent decay of MIT and CMIT concentration was best fitted to a pseudo-first order kinetics, obtaining the kinetic constants (k_{app}) listed in Table 2, which demonstrate the higher photocatalytic activity resulting by combining PS with brookite in comparison to anatase and titanates. The synergistic effect between the photocatalysts and PS was estimated by the calculation of the synergy factor (SF) for the combined systems which showed a better performance than the individual ones, as:

$$SF_{(P+PS)} = k_{A+PS} / (k_A + k_{PS}) \quad (8)$$

where k_A denotes the apparent kinetic constant of the photocatalytic reaction with TiO_2, k_{PS} the kinetic constant of the PS homogeneous reaction, and k_{A+PS} that of the combined system. A value of SF >1 indicates a synergistic effect between TiO_2 and PS for MIT/CMIT degradation while SF <1 reflects an antagonistic effect [12]. The results show a strong synergy by combining PS with B1, B2 and P25, which can be related to the effectiveness of brookite and P25 to attain the activation of PS through the transfer of e^-_{CB} from the semiconductor (Eq. (4)) and by reaction with $O_2^{\bullet-}$ (Eq. (5)). The formation of both $HO^\bullet$ and $SO_4^{\bullet-}$ radical species in UVA/TiO_2-P25/PS was previously reported in an electron paramagnetic resonance (EPR) study, in which it was also observed a prolonged lifetime of $HO^\bullet$ in the hybrid system compared to UVA/TiO_2-P25 [18]. By contrast to brookite and P25, the combination of anatase and PS had a scarce synergetic effect for CMIT degradation, even detrimental for MIT. The latter results suggest that the competition for the photons between PS and anatase is not balanced by an effective electron transfer from anatase to activate PS hence leading to a decrease in the $SO_4^{\bullet-}$ production which mostly affects to MIT degradation. As for T1 and T2, despite their higher surface area compared to TiO_2 samples and their suitable band gap value, the results show that these materials cannot be considered for photocatalytic applications neither for PS activation, hence they were discarded for the following runs.

3.3. MIT and CMIT abatement in SW

The influence of the water matrix was evaluated by spiking MIT and CMIT in SW (water parameters: COD = 18.4 mg·L^{-1}; TOC = 33.9 mg·L^{-1}; C(Cl^-) = 150 mg·L^{-1}; C(NO_3^-) = 3.1 mg·L^{-1}; C(SO_4^{2-}) = 49.0 mg·L^{-1}; C(HCO_3^-) = 258.0 mg·L^{-1}). Fig. 3 displays their concentration profiles with irradiation time, which were best fitted to a pseudo-first order decay (Table 2). Compared to ultrapure water, a significant decrease in the degradation rate was observed for PS and all titania samples in the SW individual systems, indicating an inhibitory effect of the SW constituents, which compete with the target molecules for oxidant radicals. The homogeneous PS system exhibited the highest decline in activity, more significant for MIT degradation than for CMIT. The inhibition effect of each individual ion (Cl^-, HCO_3^-, NO_3^-, SO_4^{2-}) and dissolved organic matter was evaluated in the PS system at their concentration measured in SW (Fig S3). No significant effect was observed for HCO_3^-, NO_3^-, SO_4^{2-}. However, Cl^- led to a significant increase in the reaction rate, more pronounced for MIT than CMIT, whereas humic acids had a significant detrimental effect. It has been reported that Cl^- might undergo reactions with sulfate radicals, resulting in the formation of highly oxidative chloride species able to enhance the oxidation of organic molecules [2,15]. By contrast, many studies found that natural organic matter (NOM) has a negative impact on oxidations mediated by sulfate and hydroxyl radicals due to the presence of the carboxyl and phenolic groups in humic acids, which can quickly scavenge $SO_4^{\bullet-}$, and $HO^\bullet$ [2,16]. Accordingly, the efficient scavenging of $SO_4^{\bullet-}$ by NOM in SW would counter the beneficial effect individually observed for Cl^-. Fig. 3 (A-B) also illustrates the different reaction mechanism of $HO^\bullet$ and $SO_4^{\bullet-}$ towards MIT and CMIT. The non-selective nature of $HO^\bullet$ is consistent with the similar decrease in degradation rate found for both MIT and CMIT in the individual TiO_2 systems, compared to ultrapure water. In contrast, the efficient $SO_4^{\bullet-}$ scavenging in the PS homogeneous system has a more detrimental effect on MIT degradation than on CMIT decay, consistent with the selective nature of $SO_4^{\bullet-}$, which is more prone to react with MIT than CMIT.

As observed in Fig. 3, the combination of TiO_2 and PS led to a significant enhancement in the MIT and CMIT degradation rate in SW. Table 2 displays the pseudo-first-order apparent rate constants determined for their decay and the synergistic factors between titania and PS. For the sake of clarity, Fig S4 displays a bar graph of the synergy factors. The higher performance was observed in the P25/PS and B1/PS systems, whereas the stronger synergistic effect was observed in the B1/PS system for both isothiazolinones (SF = 2.7 and 3.0 for MIT and CMIT, respectively), thereby demonstrating the superior effectiveness of brookite in activating PS compared to anatase and P25. The higher performance of B1 to activate PS reflects an efficient transfer of electrons

Table 2
Pseudo-first order kinetic constants (k_{app}) and synergy factors for the photocatalytic degradation of MIT and CMIT in Milli-Q and SW matrices.

Sample	MIT					CMIT				
	k_{app} (min^{-1}) no PS	R^2	k_{app} (min^{-1}) with PS	R^2	SF	k_{app} (min^{-1}) no PS	R^2	k_{app} (min^{-1}) with PS	R^2	SF
Milli-Q water										
B1	0.021	0.994	0.109	0.987	1.7	0.021	0.991	0.077	0.988	2.8
B2	0.017	0.994	0.087	0.952	1.4	0.017	0.995	0.075	0.966	3.1
A1	0.011	0.992	0.031	0.995	< 1	0.011	0.994	0.019	0.993	1.1
A2	0.013	0.978	0.033	0.973	< 1	0.014	0.981	0.022	0.979	1.1
P25	0.034	0.983	0.105	0.988	1.3	0.031	0.953	0.093	0.990	2.5
No catalyst	0.002	0.982	0.047	0.987	-	0.002	0.952	0.007	0.992	-
SW water										
B1	0.007	0.960	0.030	0.989	2.7	0.004	0.962	0.021	0.988	3.0
B2	0.004	0.986	0.015	0.988	1.8	0.004	0.986	0.013	0.986	1.9
A1	0.004	0.971	0.015	0.993	1.8	0.003	0.966	0.010	0.996	1.7
A2	0.003	0.990	0.008	0.998	1	0.003	0.986	0.008	0.992	1.3
P25	0.031	0.992	0.057	0.971	1.6	0.025	0.993	0.049	0.973	1.8
No catalyst	0.001	0.967	0.004	0.984	-	0.002	0.980	0.003	0.990	-

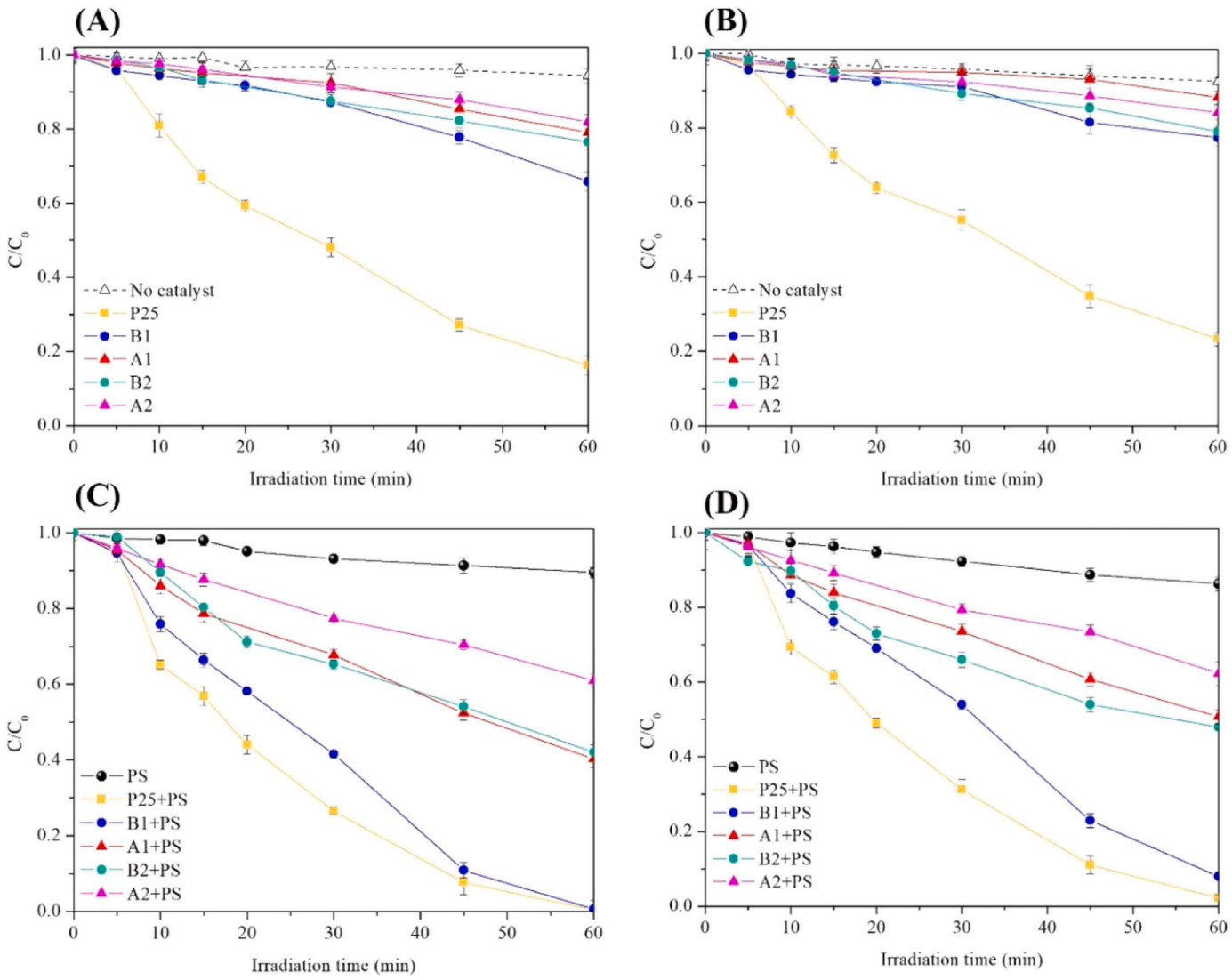

Fig. 3. Photocatalytic degradation of (A) MIT and (B) CMIT without PS addition and (C) MIT and (D) CMIT with PS addition in SW water.

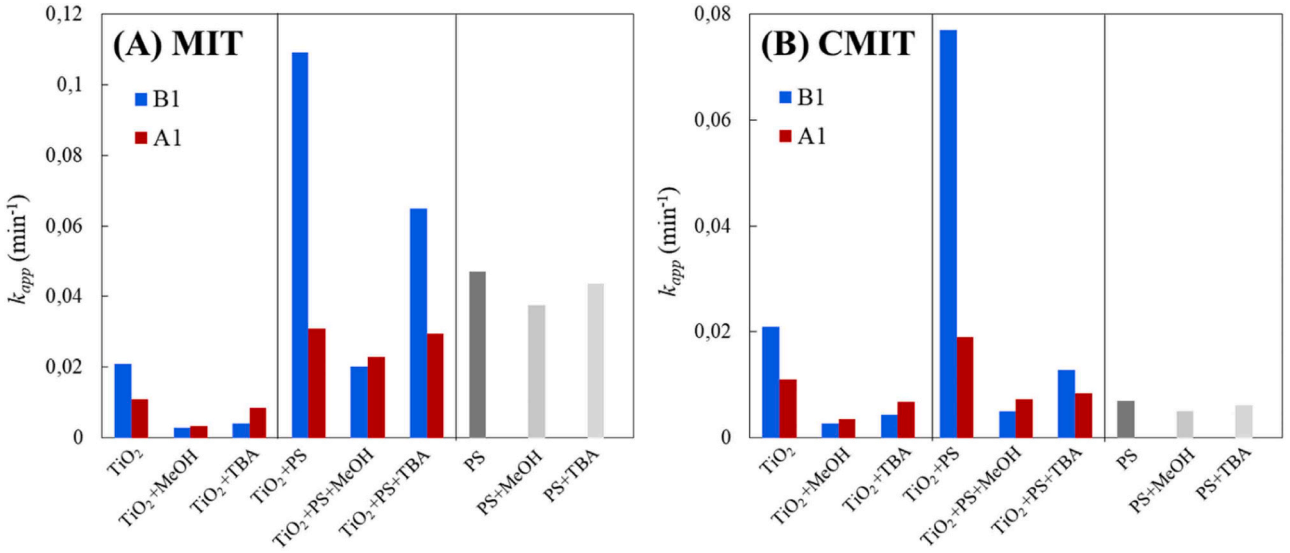

Fig. 4. Values of pseudo-first order kinetic constants obtained from scavenging experiments with individual B1, A1 and PS and combined B1/PS systems (A) MIT and (B) CMIT.

from the semiconductor to PS under UVA, which could be related to the moderate depth of the electron trap in brookite in contrast to anatase and rutile, and to a beneficial effect of defects present in the material [19]. Finally, the beneficial effect of PS/TiO_2 systems was corroborated by measuring the TOC values throughout the reaction in the SW matrix. After 120 min of irradiation, the most significant decrease in TOC was achieved in the B1/PS system (61%), followed by P25/PS (43%), in both cases substantially greater than obtained in the individual systems (8% and 27% with B1 and P25, respectively).

3.4. Scavenger tests

To investigate the contribution of $SO_4^{\bullet-}$ and $HO^{\bullet}$ to MIT and CMIT degradation the effect of the addition of 15 mM TBA and MeOH as scavengers were tested. It has been previously reported that the differences in the reactivity of $SO_4^{\bullet-}$ and $HO^{\bullet}$ with MeOH and TBA, makes it suitable their use for discriminating between the contribution of both radicals ($k_{[TBA,HO\bullet]}=6.0\times10^8\ M^{-1}s^{-1}$; $k_{[TBA,SO4\bullet-]}=4.0\times10^5\ M^{-1}s^{-1}$; $k_{[MeOH,HO\bullet]}=9.7\times10^8\ M^{-1}s^{-1}$; $k_{[MeOH,SO4\bullet-]}=3.2\times10^6\ M^{-1}s^{-1}$) [1].

Fig. 4 displays the values of the pseudo-first order kinetic constants of the reactions performed in ultrapure water with the scavengers in the individual B1, A1 and PS and combined B1/PS and A1/PS systems. In the individual brookite and anatase systems, the degradation of both MIT and CMIT was greatly inhibited by the presence of both MeOH and TBA, which could be attributed to their efficient $HO^{\bullet}$ scavenging. By contrast, a very scarce quenching effect was observed in the PS system, which would suggest excluding the role of $SO_4^{\bullet-}$ as a main oxidant in the homogeneous system. However, previous studies have reported that MIT reacts with $SO_4^{\bullet-}$ with $k_{[MIT,SO4\bullet-]}=8.0\times10^9\ M^{-1}s^{-1}$ [10]. Accordingly, the reaction of $SO_4^{\bullet-}$ with MeOH and TBA would be less favored than that of $SO_4^{\bullet-}$ with MIT, so that the alcohol molecules cannot be used as $SO_4^{\bullet-}$ quenchers in the reactions with MIT. Finally, the results with the combined B1/PS and A1/PS systems show that the quenching effect of MeOH and TBA differs between MIT and CMIT, which can be ascribed to the different reactivity of both molecules with $HO^{\bullet}$ and $SO_4^{\bullet-}$. Since MeOH and TBA preferably quench $HO^{\bullet}$ radicals, their inhibitory effect on CMIT is more pronounced than that on MIT. Also, the inhibitory effect of MeOH on MIT degradation is higher than that of TBA because of the higher reactivity of $SO_4^{\bullet-}$ towards MeOH compared to TBA.

As a summary of all the above results and some previous works [12, 20] Fig. 5 displays the plausible mechanism for MIT and CMIT degradation with TiO_2/UVA, PS/UVA and TiO_2/PS/UVA systems. Both MIT and CMIT contain electron-rich groups, such as sulfur atoms, that enable their oxidation by sulfate radicals, resulting in the formation of sulfone structures [20]. Additionally, the C═C double bond present in the structure of the target compounds is also susceptible to the $HO^{\bullet}$ attack, as previously reported [12], leading to the formation of transformation products derived from the hydroxyl attack.

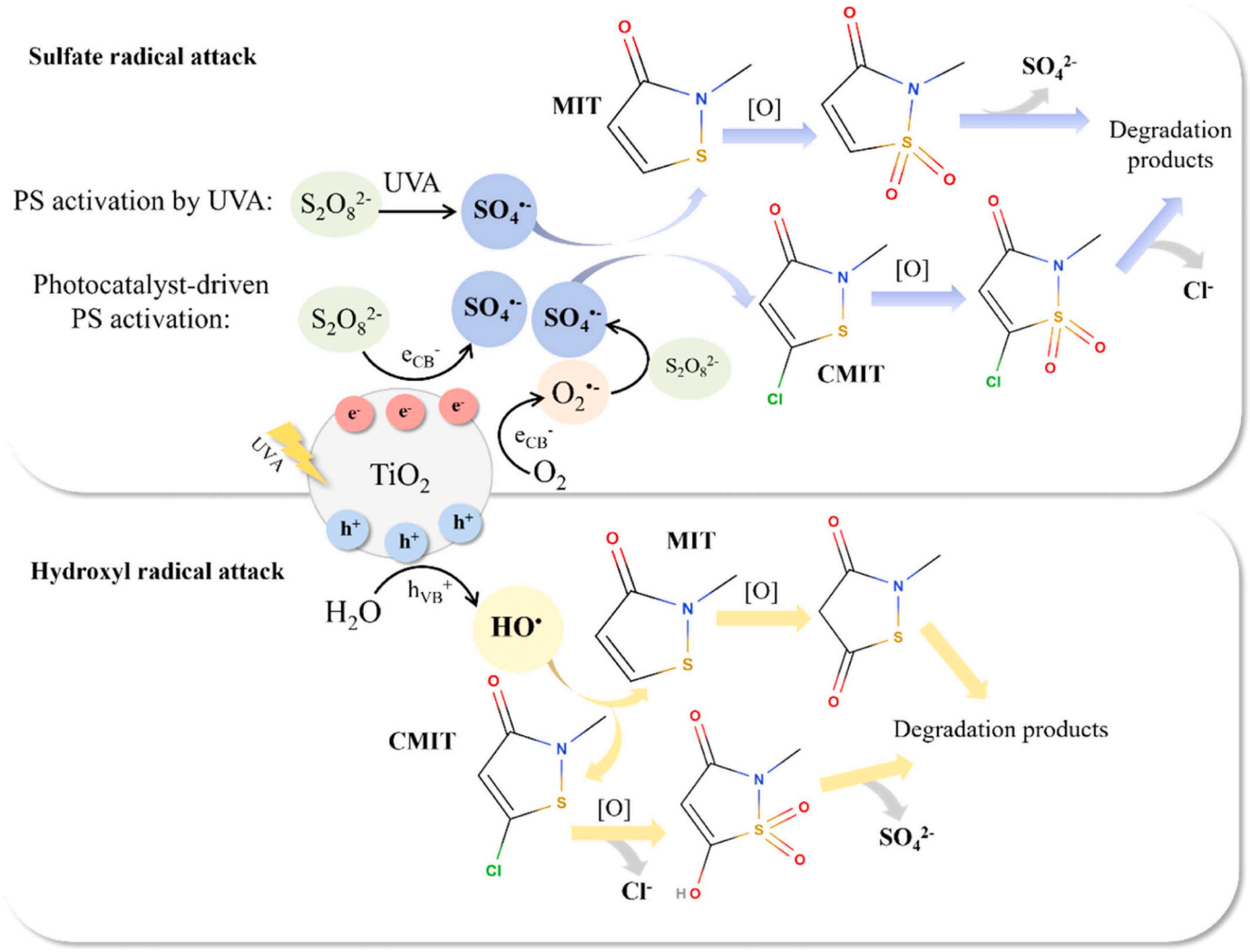

Fig. 5. Proposed mechanism for the simultaneous degradation of MIT and CMIT in UVA/TiO_2, UVA/PS and UVA/TiO_2/PS systems.

4. Conclusions

In this work, the activation of PS with brookite, anatase and titanates under UVA radiation was investigated for the removal of MIT and CMIT in ultrapure and real sewage treatment plant water. Tailoring of the desired titania phases could be successfully achieved by selection of the nature and concentration of the electrolyte, and the duration of the hydrothermal treatment used. A distinct ability in PS activation under UVA was found with TiO_2 and titanates. Titanates showed a scarce activity in the photocatalytic reactions and for PS activation under UVA, despite their suitable band gap value and higher surface area compared to TiO_2 samples. All the TiO_2 systems were active in the photocatalytic abatement of MIT and CMIT, leading the addition of PS to the improvement of MIT and CMIT degradation rates in both ultrapure water and SW matrices. The stronger synergistic effects were found between brookite and PS, which can be related to the higher effectiveness of brookite, compared to anatase, to activate of PS through the transfer of photogenerated electrons from the semiconductor. The efficiency of brookite B1 to activate PS was remarkable in the SW matrix, with strong synergy effects that might led to an increased production of oxidizing species, which allowed to overcome the inhibitory effects of the constituents present in SW. After 60 min of irradiation the degradation percentages for MIT and CMIT were >99.9% and >92%, respectively, demonstrating the potential of the combined system in SW water. The results obtained in the TiO_2 and PS individual systems with the different water matrices show a similar reactivity of $HO^{\bullet}$ towards MIT and CMIT whereas the selective character of $SO_4^{\bullet-}$ makes them more prone to react with MIT than CMIT.

CRediT authorship contribution statement

P. Gómez-Rodríguez: Investigation, Conceptualization, Writing - original draft. **R. van Grieken:** Supervision, Writing - review & editing. **M.J. López-Muñoz:** Conceptualization, Supervision, Writing - review & editing, Funding acquisition.

Declaration of Competing Interest

The authors declare that they have no known competing financial interests or personal relationships that could have appeared to influence the work reported in this paper.

Data availability

Data will be made available on request.

Acknowledgments

The authors thank the funding from Agencia Estatal de Investigación and Ministerio de Ciencia e Innovación through the AquaEnAgri project, (PID2021-126400OB-C32) and European Union's Horizon 2020 research and innovation program (Marie Skłodowska-Curie grant agreement No 101007578, SusWater project).

Appendix A. Supporting information

Supplementary data associated with this article can be found in the online version at doi:10.1016/j.jece.2024.113110.

References

[1] W.-D. Oh, Z. Dong, T.-T. Lim, Generation of sulfate radical through heterogeneous catalysis for organic contaminants removal: current development, challenges and prospects, Appl. Catal. B Environ. 194 (2016) 169–201, https://doi.org/10.1016/j.apcatb.2016.04.003.
[2] A. Derbalah, H. Sakugawa, Sulfate radical-based advanced oxidation technology to remove pesticides from water a review of the most recent technologies, Int. J. Environ. Res. 18 (2024) 11, https://doi.org/10.1007/s41742-023-00561-7.
[3] S. He, Y. Chen, X. Li, L. Zeng, M. Zhu, Heterogeneous photocatalytic activation of persulfate for the removal of organic contaminants in water: a critical review, ACS EST Eng. 2 (2022) 527–546, https://doi.org/10.1021/acsestengg.1c00330.
[4] M. Pelaez, N.T. Nolan, S.C. Pillai, M.K. Seery, P. Falaras, A.G. Kontos, P.S. M. Dunlop, J.W.J. Hamilton, J.A. Byrne, K. O'Shea, M.H. Entezari, D.D. Dionysiou, A review on the visible light active titanium dioxide photocatalysts for environmental applications, Appl. Catal. B Environ. 125 (2012) 331–349, https://doi.org/10.1016/j.apcatb.2012.05.036.
[5] M. Sabri, A. Habibi-Yangjeh, S. Rahim Pouran, C. Wang, Titania-activated persulfate for environmental remediation: the-state-of-the-art, Catal. Rev. 56 (1) (2021), https://doi.org/10.1080/01614940.2021.1996776.
[6] G.-D. Fang, D.D. Dionysiou, S.R. Al-Abed, D.-M. Zhou, Superoxide radical driving the activation of persulfate by magnetite nanoparticles: implications for the degradation of PCBs, Appl. Catal. B Environ. 129 (2013) 325–332, https://doi.org/10.1016/j.apcatb.2012.09.042.
[7] A. Di Paola, M. Bellardita, L. Palmisano, Brookite, the least known TiO_2 photocatalyst, Catalysts 3 (2013) 36–73, https://doi.org/10.3390/catal3010036.
[8] B. Ohtani, O.O. Prieto-Mahaney, D. Li, R. Abe, What is Degussa (Evonik) P25? Crystalline composition analysis, reconstruction from isolated pure particles and photocatalytic activity test, J. Photochem. Photobiol. Chem. 216 (2010) 179–182, https://doi.org/10.1016/j.jphotochem.2010.07.024.
[9] M. Ge, Z. Hu, J. Wei, Q. He, Z. He, Recent advances in persulfate-assisted TiO_2-based photocatalysis for wastewater treatment: performances, mechanism and perspectives, J. Alloy. Compd. 888 (2021) 161625, https://doi.org/10.1016/j.jallcom.2021.161625.
[10] Z.-W. Yang, W.-L. Wang, M.-Y. Lee, Q.-Y. Wu, Y.-T. Guan, Synergistic effects of ozone/peroxymonosulfate for isothiazolinone biocides degradation: kinetics, synergistic performance and influencing factors, Environ. Pollut. 294 (2022) 118626, https://doi.org/10.1016/j.envpol.2021.118626.
[11] M.J. López-Muñoz, A. Revilla, G. Alcalde, Brookite TiO_2-based materials: synthesis and photocatalytic performance in oxidation of methyl orange and As(III) in aqueous suspensions, Catal. Today 240 (2015) 138–145, https://doi.org/10.1016/j.cattod.2014.05.008.
[12] P. Gómez-Rodríguez, P. Calza, D. Fabbri, C. Medana, R. van-Grieken, M.-J. López-Muñoz, Photocatalytic degradation of methylisothiazolinone in water by TiO_2 and TiO_2/persulfate systems with simulated solar radiation, Catal. Today (2023) 413–415, https://doi.org/10.1016/j.cattod.2022.11.003, 113942.
[13] W. Hu, L. Li, G. Li, C. Tang, L. Sun, High-quality brookite TiO_2 flowers: synthesis, characterization, and dielectric performance, Cryst. Growth Des. 9 (2009) 3676–3682, https://doi.org/10.1021/cg9004032.
[14] J. Zhang, Y. Nosaka, Mechanism of the OH radical generation in photocatalysis with TiO_2 of different crystalline types, J. Phys. Chem. C 118 (2014) 10824–10832, https://doi.org/10.1021/jp501214m.
[15] W. Huang, A. Bianco, M. Brigante, G. Mailhot, UVA-UVB activation of hydrogen peroxide and persulfate for advanced oxidation processes: efficiency, mechanism and effect of various water constituents, J. Hazard. Mater. 347 (2018) 279–287, https://doi.org/10.1016/j.jhazmat.2018.01.006.
[16] J. Lee, U. von Gunten, J.-H. Kim, Persulfate-based advanced oxidation: critical assessment of opportunities and roadblocks, Environ. Sci. Technol. 54 (2020) 3064–3081, https://doi.org/10.1021/acs.est.9b07082.
[17] P. Neta, V. Madhavan, H. Zemel, R.W. Fessenden, Rate constants and mechanism of reaction of sulfate radical anion with aromatic compounds, J. Am. Chem. Soc. 99 (1977) 163–164, https://doi.org/10.1021/ja00443a030.
[18] M.G. Antoniou, I. Boraei, M. Solakidou, Y. Deligiannakis, M. Abhishek, L. A. Lawton, C. Edwards, Enhancing photocatalytic degradation of the cyanotoxin microcystin-LR with the addition of sulfate-radical generating oxidants, J. Hazard. Mater. 360 (2018) 461–470, https://doi.org/10.1016/j.jhazmat.2018.07.111.
[19] J.J.M. Vequizo, H. Matsunaga, T. Ishiku, S. Kamimura, T. Ohno, A. Yamakata, Trapping-induced enhancement of photocatalytic activity on brookite TiO_2 powders: comparison with anatase and rutile TiO_2 powders, ACS Catal. 7 (2017) 2644–2651, https://doi.org/10.1021/acscatal.7b00131.
[20] X. Li, Z. Li, Z. Xing, Z. Song, B. Ye, Z. Wang, Q. Wu, UV-LED/P25-based photocatalysis for effective degradation of isothiazolone biocide, Front. Environ. Sci. Eng. 15 (2021) 85, https://doi.org/10.1007/s11783-020-1379-x.